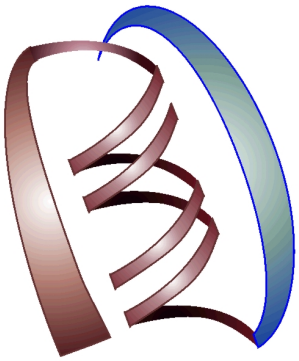

BIOMEDICAL
ENGINEERING

Carnegie Mellon University

2019 Biomedical Engineering
Summer Undergraduate Research Symposium

August 1, 2019
10:00 AM to 1:00 PM
Scott Hall 4N200

August 2, 2019
10 AM to 12:30 PM
Scott Hall 4N200

Biomedical Engineering at Carnegie Mellon University
Biomedical engineering education at Carnegie Mellon reflects the belief that a top biomedical engineer must be deeply trained in both a traditional engineering practice and biomedical sciences. The unique additional major program leverages extensive collaborations with sister departments in the College of Engineering and with major medical institutions in Pittsburgh. This collaborative approach, combined with a rigorous engineering education, confers unique depth and breadth to the education of Biomedical Engineering graduates.

Biomedical Engineering Summer Undergraduate Research Program (BME SURP)
This program allows students to spend a ten-week period on a project that combines translational research and clinical exposure at a local medical center. Hundreds of students have participated in BME-SURP since its introduction in 1980. The experience has played a major role in helping students choose their career paths and obtain positions in industrial or academia. This program is supported by grants from the CMU College of Engineering This program is supported by grants from the CMU College of Engineering and the CMU University Research Office (URO).

Carnegie Heart Program
The Carnegie Heart Program is a collaborative effort between the Biomedical Engineering Department at Carnegie Mellon University and the Allegheny Health Network. The purpose of this program is to develop biomedical engineers who can apply their education toward new technologies for clinical cardiovascular medicine. In addition to students' experience in a laboratory setting, students will shadow cardiovascular clinicians at Allegheny General Hospital one day approximately every two weeks. This program is supported through a grant from the American Heart Association.

Presentation Schedule

August 1, 2019 (Thursday)
10:00 AM: Sean Pereira (BME SURP/URO)
10:15 AM: Vivenne Pham (BME SURP/URO)
10:30 AM: Sanjana Shah (BME SURP/URO)
10:45 AM: Nathan Roblin (BME SURP/URO)
11:00 AM: Mairin (Molly) Flanagan (BME SURP/URO)
11:15 AM: Madeline Evans (BME SURP/URO)
11:30 AM to 11:45 AM: BREAK
11:45 AM: Stella Getz (BME SURP/URO)
12:00 PM: Isabel Joyce (BME SURP/URO)
12:15 PM: Nihal Sivakumar (BME SURP/URO)
12:30 PM: Xining Gao (Carnegie Heart)
12:45 PM: Lunch and Cake!

August 2, 2019 (Friday)
10:00 AM: Juan Cortes (BME SURP)
10:15 AM: Augustine Duffy (BME SURP)
10:30 AM: Olivia Olshevski (BME SURP)* and Julia Salerno (BME SURP)*
10:45 AM: Bryant Chung (Carnegie Heart)
11:00 AM to 11:15 AM: BREAK
11:15 AM: Sarah Hargett (Carnegie Heart)
11:30 AM: Mimi (Xinyi) Li (Carnegie Heart)
11:45 AM: GianCarlo Seixas (Carnegie Heart)
12:00 PM: Lunch and Cake!

Isabelle Chickanosky (BME SURP/URO) presented at a separate time due to a conflict.

* Supported by BME Design funding from Medtronic, Inc. Bayer, and ALung

Screening Platform for Studying Human Obesogenic Compounds

Sean R. Pereira[1], Mallory D. Griffin[1], Megan K. DeBari[1], and Rosalyn D. Abbott[1]
[1]Carnegie Mellon University, Pittsburgh, PA

Introduction: Many researchers and doctors attribute increased consumption of highly caloric foods together with physical inactivity as the driver of the metabolic diseases such as Obesity and Type II Diabetes (T2D) [2]. Additionally, shifts in population genetics are also a driver in such metabolic diseases. However, in the last several decades, there has been a dramatic increase in obesity and T2D. With over a third of the US population being characterized as Obese in 2011 and with number of those afflicted with diabetes doubling these factors alone cannot account for the increased rate of metabolic diseases in such a short span [1]. Evidence has suggested that endocrine disrupting chemicals, termed obesogens, can disrupt metabolic pathways in adipose tissue. With the rise of environmental contaminants classified as obesogens, there is a need to understand the pathogenic impact made by these chemicals A diverse array of compounds have been identified already but there is still a need to understand what new synthetic compounds pose a threat to metabolic health.

Materials and Methods: 2D and 3D systems were compared to determine the most physiologically relevant system. Cells were exposed to known obesogens: tributyltin (TBT) and bisphenol A (BPA) and characterized for obesogenic outcomes. For the 2D studies, the hES-MSCs were seeded onto well plates coated with 0.1% ultrapure gelatin water. And for the 3D studies, the hES-MSCs were encapsulated in Hyaluronic acid (HA) based Hydrogels and placed in well plates. Afterwards hES-MSCs were cultured in maintenance media with Obesogens/ /Controls treatment for 14 days. Cells and Media were concurrently used in AdipoRed staining, intracellular triglyceride accumulation, glycerol secretion, DNA content, and qRT-PCR. Lastly, the data collected will be utilized in creating a supervised machine learning model (SVM) to create a Model. This model will be used to characterize the unknows as either obesogenic or non-obesogenic compounds.

R**esults and Discussion:** hES-MSCs were differentiated in 2D and 3D cultures in order to evaluate which physiological system would be the most predictive. Figure 1 shows images of cells in 2D culture and 3D culture. While 2D hESC intracellular triglyceride data suggested that BPA promotes secretion rather than storage of lipids (inconsistent with the literature where BPA increased the size of adipocytes in mice in vivo), the 3D hESC platform showed that the addition of obesogens increased lipogenesis. This is likely due to differences between the environment provided by the 2D environment compared to the 3D environment. The 3D environment is more similar to the *in vivo* environment, providing support for the adipocytes and accommodating lipid accumulation.

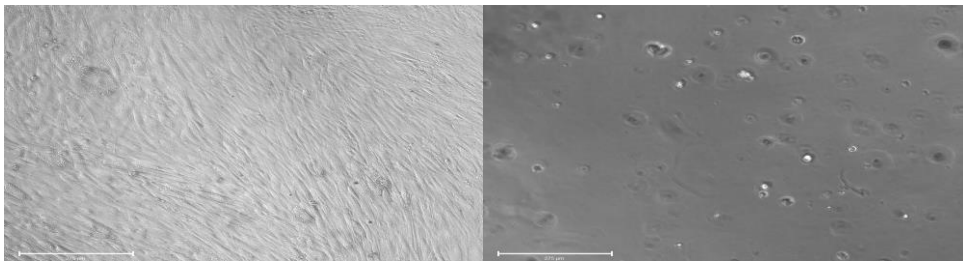

Figure 1. (I) hES-MSCs seeded onto well plates coated with 0.1% ultrapure gelatin water. **(II)** hES-MSCs seeded onto well plates encapsulated in HA based Hydrogels.

Conclusions: Moving forward, 3D environments will be used as a screening platform for obesogenic effects. Further research is needed to test potential obesogens in this 3D environment to create a viable computational model to successfully predict whether unknown chemical compounds are obesogenic or non-obesogenic.

Acknowledgements: This work was partially supported by the Small Undergraduate Research Grants (SURG) program.

References:

1. S.N. Bhupathiraju, *Circ Res*, 2016, vol. 118, no. 11, pp. 1723-1735
2. S.M. Regnier, *Biochimica Et Biophysica Acta (BBA)*, 2014, vol. 1842, no. 3, pp. 520-533
3. R.Y. Wang, *Annals of Biomedical Engineering*, 2016, vol. 45, no. 7, pp. 1807–1818

Engineering Tissue by 3D Printing

Authors: Vivienne Pham

Introduction: The demand for organs exceeds the number of organs available for transplantation. As a result, there are over 100,000 patients on the organ transplant list and 20 people die each year waiting for an organ. One method in which tissue engineering is attempting to combat this problem is with 3D printed ECM scaffolds. One problem with seeding cells to the scaffolds is low cell adhesion, particularly with cardiomyocytes. We investigated a method to improve cell adhesion using click chemistry and DNA hybridization. Click chemistry is used to describe fast reactions between substrates and specific biomolecules. By conjugating one strand of DNA to a scaffold and the other strand of DNA to the cells, the DNA strands can hybridize when the cells are placed on the scaffold.

Materials and Methods:

Because a common material for 3D printed ECM scaffolds is collagen I, we made collagen I (rat tail) gels to model a 3D scaffold. The azide functional group was first conjugated to a collagen gel with the reagent Azide-PEG4-NHS Ester. A control gel was treated with 10% DMSO. Azide conjugation to the collagen was tested with DBCO-488. The strand of DNA (V1D1) was then conjugated to the azide labeled collagen gel using the reagent DBCO-V1D1. V1D1 conjugation to azide labeled collagen was tested with V1D2-6FAM. HUVEC cells were sugar fed ManNAz in order to metabolically label the cells with the azide group. The complementary strand of V1D1, which is V1D2, was conjugated to the cells using DBCO-V1D2. The cells were then added to the gels and washed thoroughly. The gels were lastly stained with Hoechst and fluorescein phalloidin and imaged on an automated microscopy system.

Results and Discussion:

The positive azide group and the negative 10% DMSO group showed significant difference in green fluorescence after being treated with DBCO-488. The positive and negative groups showed significant difference in green fluorescence after being treated with V1D2-6FAM. The V1D1 conjugated azide labeled gel showed significantly more cells attached than the control group.

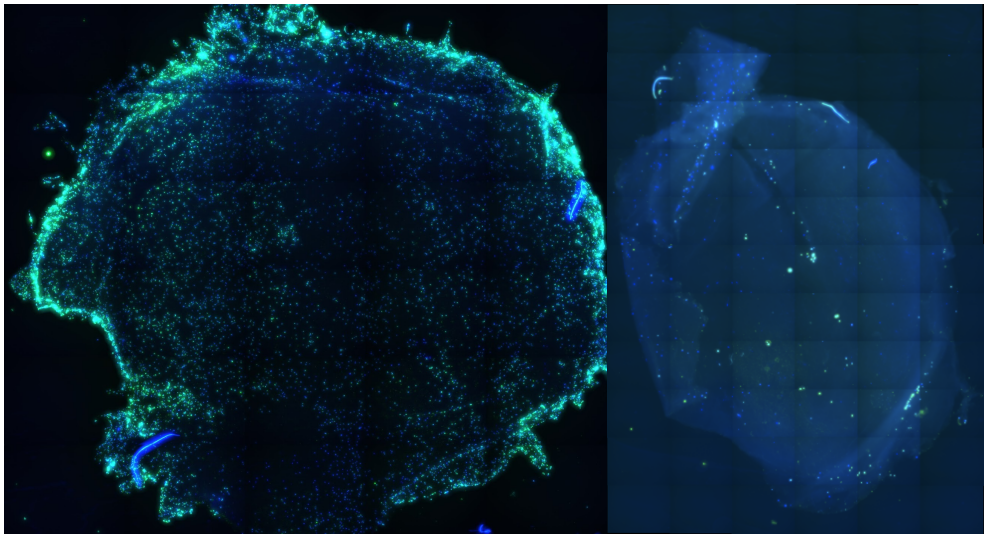

Figure 1. Positive group (left) show significantly more cell adhesion than the control group (right).

Conclusions: The results demonstrate that the use of click chemistry and DNA hybridization can improve cell adhesion to a collagen scaffold. Future work entails conjugating cardiomyocytes to Dr. Feinberg's 3D printed scaffold.

Acknowledgements: I would like to acknowledge Dr. Charlie Ren, Dr. Adam Feinberg, Piyumi Wijesekara, and Yunhui Xing for their help with this project. I would like to thank the BME department at CMU for funding my project.

Utilizing Fibronectin-Based Nanomechanical Sensors to Measure Strain on Myoblasts

Sanjana Shah[1], Daniel Shiwarski[1], Adam Feinberg[1,2]
Departments of Biomedical[1] and Materials Science[2] Engineering, Carnegie Mellon University, Pittsburgh, PA

Introduction: To achieve physiological contractile forces, cardiomyocytes require anisotropic alignment. Using micropatterning-based approaches, it is possible to engineer aligned cardiomyocytes; however, evaluating their mechanical function during myogenesis is technically challenging. Traditionally, mechanical forces are difficult to quantify in living tissue and have been limited to 2D traction forces [1]. We have developed a novel fibronectin-based nanomechanical biosensor (NMBS) for direct measurement of 3D tissue level strain. The NMBS is an extracellular matrix protein lattice structure that acts as a fiduciary marker to directly visualize dynamic cellular strain over time. By utilizing the NMBS and C2C12 mouse myoblast cells, we will measure mechanical strain during C2C12 myogenesis of cells grown isotropically and on anisotropically patterned fibronectin lines to improve our understanding of the mechanobiology driving muscle cell differentiation.

Materials and Methods: The NMBS pattern is drawn in AutoCAD and then transferred to a transparent photomask, which is exposed to UV light to create a photoresist patterned glass wafer. Polydimethylsiloxane (PDMS) is added over the wafer to create a stamp, which is then coated with fluorescently-labeled fibronectin. The fibronectin-coated stamp is microcontact printed onto a glass coverslip coated with a Poly(N-isopropylacrylamide) (PIPAAm) [2]. For application to cell monolayers, the stamped coverslips are placed on top of a gelatin carrier, and water is added to dissolve the sacrificial PIPAAm substrate releasing the stamped NMBS and transferring it to a gelatin carrier. Finally, the gelatin carrier is placed onto a cell monolayer and incubated at 37°C to melt the gelatin and transfer the NMBS on to the cells. Strain is measured via fluorescence imaging NMBS deformation over time. Changes in length of each segment of the NMBS are used to calculate the strain via a custom MATLAB code. C2C12s are cultured on isotropic fibronectin-coated coverslips or on micropatterned fibronectin lines to create cell alignment. C2C12 cells are passaged at 80% confluence for plating onto glass coverslips and patterned fibronectin PDMS coverslips [3].

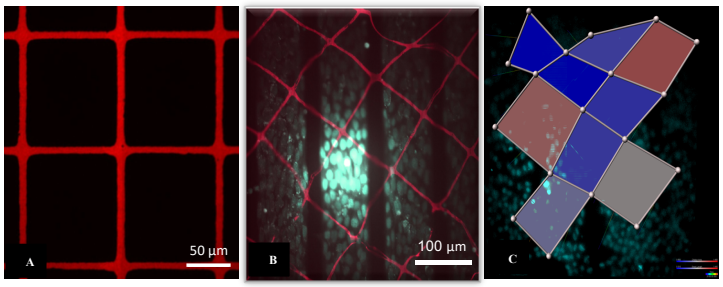

Figure 1. NMBS fabrication (left), NMBS application to aligned cells grown on anisotropically patterned fibronectin lines on PDMS (middle) and strain map of the aligned cells after 24 hours (right).

Results and Discussion: The NMBS was fabricated in two sizes, 100 µm width x 100 µm length x 10 µm fiber thickness (Figure A) and 50 x 50 x 10 µm. These patterns were applied to non-aligned and aligned cells (Figure B) and a strain map was created (Figure C). The 50 x 50 x 10 µm NMBS provided the required resolution for evaluating the strain field. The maximal tensile and compressive strain for the aligned cells was 1.44 and 0.515 whereas for the non-aligned cells, the maximal tensile and compressive strain was 1.48 and 0.660. Despite experiencing similar strain magnitudes, the aligned cells showed directional strain preference toward their alignment.

Conclusions: As shown here, the NMBS can be applied to cell monolayers to track cell movement and myoblast elongation over time. We have begun to measure the strain patterns of cells grown isotropically and cells grown on anisotropically patterned fibronectin lines. In the future, we will continue to map strain patterns for aligned and non-aligned cells while additionally performing functional measurements via fluorescence calcium imaging and contractile force quantification.

References: [1] Munevar S, Wang Y, Dembo M. Traction Force Microscopy of Migrating Normal and H- Ras Transformed 3T3 Fibroblasts. Biophysical Journal. April 01, 2001 **[2]** Feinberg AW, Parker KK. Surface- Initiated Assembly of Protein Nanofabrics. Nano Letters. May 20, 2010 **[3]** Duffy RM, Sun Y, Feinberg AW. Understanding the Role of ECM Protein Composition and Geometric Micropatterning for Engineering Human Skeletal Muscle. Ann Biomed Eng. June 01, 2017

Flexible Electronic Biosensors for Monitoring Cardiac Output

Nate Roblin, Bryant Chung, Adrian Johnson, Chenchen Mou, Dr. Christopher Bettinger - CMU Dept. MSE/BME

Introduction: After open heart surgery, cardiac function must be constantly monitored to ensure there are no complications. The current method for involves a Swan-Ganz catheter, a sensing stent that is inserted into the heart and major arteries. However, an internal sensor can puncture cardiovascular tissue or lead to clotting, and this type of sensor would have to be removed after a short period of time. This study aims to supplant the Swan-Ganz catheter by creating a strain gauge capable of measuring arterial expansion to monitor blood flow from the external surface of major arteries, via the piezoresistive nature of conducting materials such as aqueous ions and metals[1]. A conductive iron-catechol hydrogel will be used for adhesion to tissue while gold traces will be used for measuring resistance data. Strain on the sensor caused by blood flow will cause the ions to be further separated and microcracks to form in the gold structures, increasing the resistance by decreasing conduction.

Materials and Methods: This study used gold structures nanofabricated on silicon wafers coated with polyacrylic acid (PAA), in addition to ($[PEG\text{-}Cat]_4$) polymer samples, produced by graduate student Chenchen Mou. Tris buffer (created using tris particles and distilled water) was used to create polymer and iron chloride solutions. Polymer solution was then applied onto the wafer containing gold traces, and an equal volume of iron chloride solution was added to induce crosslinking to produce a hydrogel. The hydrogel then dissolved the PAA to allow the gold to be transferred onto the hydrogel surface, creating a sensor device. The sensor was then removed and adhered onto PDMS (to replicate mechanical properties of cardiovascular tissue). Strain was incrementally applied to the sensor via the PDMS, and resistance across the sensor was recorded at each stage with a multimeter.

Results and Discussion: Preliminary testing has yielded several positive results. Upon refinement of the formulation used to produce the iron-catechol hydrogel, it was found that using a 0.4 ratio of Fe^{3+} ions to catechol with 40mM ($[PEG\text{-}Cat]_4$) polymer solution produced a hydrogel that could transfer print gold structures onto its surface. Prototypes produced using this method were used to determine the range of linearity and sensitivity of the sensor. It was determined that this model sensor has a linear relationship between strain and relative resistance for strains of up to 22.1%, and the sensing sensitivity for this device was determined to be 3.18[1] (Figure 1).

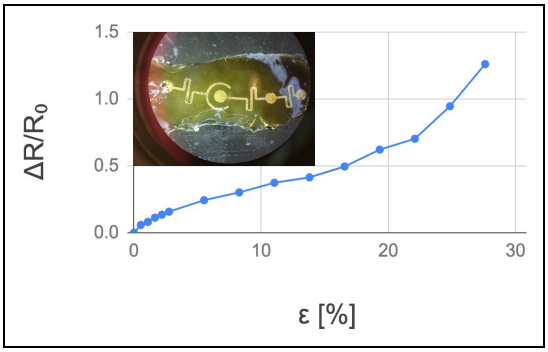

Figure 1: This plot shows the relationship between the strain (ε) applied and the measured relative resistance ($\Delta R/R_0$, where R_0 is the initial resistance) across the sensor prototype (smaller image set within figure). A linear relationship was observed between strain and $\Delta R/R_0$ for strains of up to 22.1%, at which point the relationship started to become exponential in nature. The sensing sensitivity (or gauge factor) of this prototype was determined by finding the slope of the linear region using fractional strain, 0.70/0.22087 = 3.18.

Conclusions: Data from preliminary testing indicates that the piezoresistivity of aqueous iron ions and the gold traces should be sufficient for measuring arterial expansion. Development of prototype sensors indicated that this sensor can be feasibly fabricated. Further testing will be conducted to increase the range for linear correlation between strain and relative resistance, and then animal trials will be performed with sensors on major arteries.

Acknowledgements: I would like to acknowledge Dr. Christopher Bettinger, Chenchen Mou, Bryant Chung and Adrian Johnson for contributions, as well as the URO and Biomedical Engineering department for my funding.

References:

[1] Amjadi, M, et al. *Adv. Funct. Mater.* **2016**, 26 (11), 1-21, doi:10.1002/adfm.20150475.

3D Printing of Biofabricated Lungs with Sacrificial Inks

Authors: Madeline Evans (ChemE), Molly Flanagan (MSE/BME)

Introduction:

Chronic lung diseases affect over 15 million people and rank as the 4th-leading cause of death in the United States. Current long-term treatment methods like non-invasive ventilation and lung transplants help to alleviate symptoms of these diseases but fail to meet full support standards: Non-invasive methods like oxygen supplementation cannot provide the full need of gas exchange within the lung. Transplant demand of lungs well exceeds the available supply and requires constant immuno-suppression to prevent the reduction of gas exchange with rejection. To address this deficiency in adequate treatment, we propose a new method of 3-D printing a fully biocompatible (i.e. fabricated with natural materials to prevent negative immune response) lung to supplement a patients' natural gas exchange function. Our goal is to design a method to 3D print sacrificial ink networks into collagen, the structural protein in many of the body's connective tissues.

Materials and Methods:

We selected several biocompatible ink candidates to investigate further: carbohydrate glass, poly-4-hydroxybutyrate (P4HB), sodium alginate, and Pluronic F-127. For each material, various literature sources and experimental experts were consulted to understand their printability. We considered the mechanical, chemical, and thermal properties of each. We determined that out of the selections, sodium alginate and Pluronic had the most suitable properties for our application.

Results and Discussion:

All inks were encouraging materials but ultimately P4HB and carbohydrate glass were disregarded. We found that P4HB is used as a fiber-forming surgical meshes and dissolvable sutures, however it has not yet been used for printing purposes or basic extrusions. It also would not work as a sacrificial material because it degrades in vivo over the course of several weeks. Analogously, despite being easily dissolvable in water, carbohydrate glass needed to be kept far too hot to manipulate through a syringe which is unsuitable for 3D printing.

Pluronic F-127 could be printed at room temperature with a high degree of precision, and we found that adding high molecular weight PEO improved this precision. We learned that Pluronic F-127 is thermoreversible, meaning it liquefies at colder temperatures and gels at higher temperatures. Because of this, it could be heated along with collagen to crosslink/gel both components, then cooled to remove the Pluronic and leave the collagen in tact. We found that sodium alginate could be crosslinked easily and precisely with $CaCl_2$ and the addition of a chelator to separate the calcium makes degradation and removal straightforward.

Conclusions:

The findings suggest that Pluronic F-127 and sodium alginate have the most suitable properties for serving as the sacrificial ink for 3D fabricating a collagen structure. Due to its thermoreversibility, Pluronic F-127 should be heated to 23^{o} C to initiate gelation before printing. Once printed into collagen, the temperature should be increased to 37^{o} to crosslink the collagen components. The entire structure should then be cooled to liquefy and wash out the Pluronic. If using alginate instead, $CaCl_2$ should be added to its support bath of collagen to simultaneously crosslink both components during extrusion. The temperature should be raised to 37^{o} to further crosslink the collagen, then a chelator should be introduced to degrade and remove the alginate.

Acknowledgments: We would like to express our gratitude to Dr. Keith Cook and Erica Comber for their guidance, as well as the Undergraduate Research Office and the Bioengineered Organs Initiative for funding.

References:

[1] T. J. Hinton. Three-dimensional printing of complex biological structures, *Science* (2015).

[2] Derakhshanfar, S. 3D bioprinting for biomedical devices and tissue engineering, *Bioactive Materials* (2018).

[3] Martin, D.P. Medical applications of poly-4-hydroxybutyrate. *Biochemical Engineering Journal* (2003) 97–105.

[4] Kolesky, D. B. 3D Bioprinting of Vascularized, Heterogeneous Cell-Laden Tissue Constructs, *Advanced Materials* (2014).

The Effect of Peptide Modification on the Electrical Properties of Graphene

Authors: Stella Getz, Daniel San Roman, Anna Kalmykovs, Tzahi Cohen-Karni

INTRODUCTION

Graphene is a single 2-dimensional layer of sp2 -hybridized carbon atoms which exhibits transparency, mechanical strength, flexibility, and high electrical conductivity. [1] Mustata *et al*. developed methods for graphene modification with charged peptides – which may open promising applications for bioelectrochemical sensors in the form of peptide-modified graphene field effect transistors (gFETs). [2] This project extends prior research by using gFETs to characterize the effects of peptide modification on graphene's electrical properties. We improve upon traditional doping methods (insertion of non-carbon atoms in graphene lattice) by attaching peptides at graphene's surface that preserve the carbon lattice structure while still producing desirable electrical properties. We will modify graphene with peptides Ac-$(KF)_4$-NH_2 (KF) and Ac-$(EF)_4$-NH_2 (EF), separately, and characterize the resultant changes in electrical properties with respect to pristine graphene.

MATERIALS AND METHODS

We synthesize single-layer graphene using Low Pressure Chemical Vapor Deposition (LPCVD) and transfer this graphene onto an Si/SiO2 (285nm) substrate patterned with metal interconnects that form electrical contacts between each graphene channel. We follow previously established methods for peptide modification [3]; the gFETs are incubated for 30 minutes in peptide solution, allowing peptide self-assembly on the graphene.

We confirm graphene modification using contact angle measurement, Atomic Force Microscopy (AFM), X-ray Photoelectron Spectroscopy (XPS), and Raman spectroscopy to compare surface characteristics of pristine and peptide-modified gFETs. These methods respectively inform us on the hydrophilicity, topography, elemental composition, and structure of our surface.

Finally, we electrically characterize our devices by sweeping the gate voltage (Vg) and plotting the source-drain currents (Isd) to determine the Dirac points (Vg at which the Isd is at its minimum) of pristine, EF-modified, and KF-modified gFETs. A shift in the Dirac point indicates graphene doping, and the direction of the shift indicates the type of doping (n-type or p-type).

RESULTS AND DISCUSSION

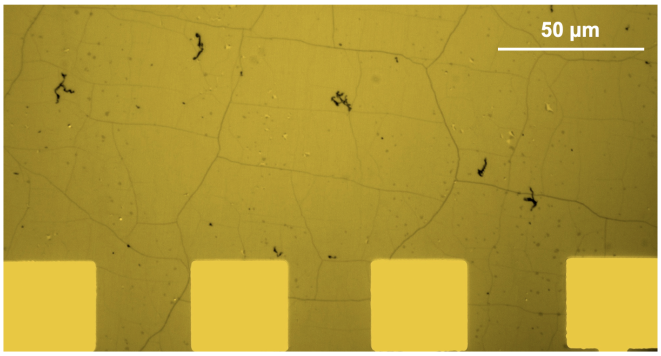

Figure 1. Graphene on Si/SiO_2 substrate, patterned with metal pads (lighter squares) and interconnects, device region, 50x magnification

Figure 1 reveals darker lines across the chip's surface in patterns characteristic of graphene grain boundaries. LPCVD graphene is synthesized starting from multiple graphene grains which grow outward until they intersect, forming visible boundaries.

We see grain boundaries in all optical images of our recent chips' device regions. The presence of grain boundaries in our optical images demonstrate that we successfully transferred graphene onto our chips, meaning we can proceed to finish patterning our chips to make our final gFET devices.

CONCLUSIONS

Our optical images show that we have both succeeded in synthesizing single-layer graphene through LPCVD and that we have succeeded in transferring that graphene onto our chips. Having established and implemented these foundational device-creation processes, we may proceed to modify, characterize, and compare our devices. After peptide-modifying a subset of devices, we will electrically characterize all devices to determine and document the effects of the two peptide modifications on graphene's electrical properties.

[1] Geim, A. K. *et al.*, *Graphene: Status and Prospects*, Science, 2009, 1530-1534
[2] Mustata *et al., Graphene Symmetry Amplified by Designed Peptide Self-Assembly*, Biophysical*Journal*, 2016, 2507-2516
[3] Hayamizu *et al.*, *Bioelectronic interfaces by spontaneously organized peptides on 2D atomic single layer materials*, Scientific Reports, 2016, 33778

Wet Spinning of Genipin-Doped Poly(ethylene-co-vinyl alcohol) Fibers for use in Embolization Procedures

Isabel Joyce, Malia Okamura, Dr. Christopher Bettinger

Introduction: Brain aneurysms are a common cause of strokes. An aneurysm is formed from a dilation in a blood vessel. Instead of the blood flowing straight through the blood vessel, the bulge causes the flow to be disrupted. The current method used to prevent rupturing is to insert a platinum coil into the dilation. The insertion of this coil helps form a clot, which allows the blood to flow straight through the blood vessel again. While successful in many instances, this procedure fails between 20-30% of the time due to recanalization of the nascent clot. Here we propose a genipin-eluting polymer-based embolization device. The polymer fiber itself will induce clotting and closure of the aneurysm and deliver genipin locally to the aneurysm sac. Genipin, a small molecule crosslinking agent, will chemically and mechanically stabilize the nascent clot to reduce the likelihood of recanalization. Here, we report details about fiber production using wet spinning.

Materials and Methods: The polymer fibers were made by wet spinning[1]. Briefly, a solution of poly(ethylene-*co*-vinyl alcohol) (PEVA) and genipin in dimethyl sulfoxide (DMSO) solvent was prepared. The solution was injected at a rate of 20mL/h into a coagulation bath composed of double-distilled water (ddH_2O). The samples were then analyzed using FTIR-ATR and UV-Vis analysis techniques. The FTIR-ATR helped determine whether or not genipin was in the sample, by comparing the peaks of the carbonyl and carbon-hydrogen bond wavelengths. The UV-Vis was used to determine how much genipin was in each sample.

Results and Discussion: Through varying the percent of polymer used, the amount of genipin, the flow rate of the fiber being released from the sample, the size of the needle, and the method of inserting the genipin, we've determined a set of parameters that optimize the amount of genipin in the sample. Decreasing the percent of polymer, increasing the needle size, increasing the flow rate, and increasing the amount of genipin in the sample all result in a larger genipin to polymer ratio.

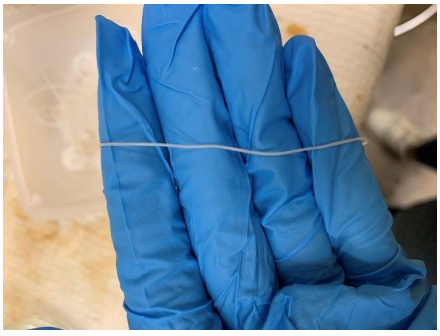

Figure 1. The image shown is a polymer fiber laced with genipin. Though each fiber may alter in size and texture, all the fibers we've produced look something like the one shown. The fibers are as long as we want them to be and have a width of about ?????.

Conclusions: Wet spinning is a viable method to create genipin-loaded PEVA fibers for potential use as embolization devices for the treatment of intracranial aneurysms. Future work will focus on quantifying genipin loading and exploring alternative scalable manufacturing techniques for fiber production such as extrusion.

Acknowledgements: I would like to thank the URO for giving me the opportunity to perform this research this summer.

References: Puppi D., Chiellini F, *Society of Chemical Industry*, 2017, doi: 10.1002/pi.5332

Adapting Techniques used in Laser Powder Bed Fusion to Create Biocompatible Parts via Binder Jetting

Authors: Nihal Sivakumar[1], Samuel Passell[1], Amir Mostafaei[1], Jerard Gordon[1], Anthony Rollett[1]
[1]Carnegie Mellon University, Department of Materials Science and Engineering, Pittsburgh PA

Introduction

Additive Manufacturing (AM) is a relatively novel way to assemble parts by 3D printing. Currently, metal AM parts have been revolutionizing the aerospace, automotive, and biomedical industries, typically by fusing metal powder into the desired part shape. Laser Powder Bed Fusion (LBPF), Electron Beam Melting (EBM), and binder jetting have been proven to produce strong, dense builds. Our overall goal is to build biocompatible implants with Ti-6Al-4V (Ti64) using EBM and Co-Cr using binder jetting and inducing porosity channels in each build to mimic mechanical properties of bones to stimulate bone tissue formation. Our current goal for the summer is to be able to analyze the microstructure of two nickel alloys, Inconel 718 and CMSX-4, and be able to replicate the method to later examine the efficacy of binder jetting towards creating highly porous parts.

Materials and Methods

We analyzed 29 laser melt pool tracks in CMSX-4 and 6 LBPF builds in Inconel 718 in order to understand how to analyze their microstructure and porosity. Each melt pool track and build had different laser power and velocities, which affected the microstructure and porosity. The two densities were then compared and determined to be similar to the expected density, indicating that these measurement methods were accurate. This same technique will be used when printing Ti64 or Co-Cr samples using binder jetting to verify that binder jetting can produce parts with optimal porosity levels.

Results and Discussion

We were able to gain significant data to demonstrate our ability to accurately calculate porosity and analyze microstructures. The porosity measurements for 718 proved our hypothesis- we expected all 6 samples to have porosity levels less than .5%, and the data supports our results as shown in figure 1. We were able to identify the lowest porosity samples having 285W and either 600 or 800 mm/s, and either increasing the speed or power of the laser from this will result in increased porosity levels. The above method was able to successfully determine the densities of the Inconel 718 samples and can be replicated for any other material used.

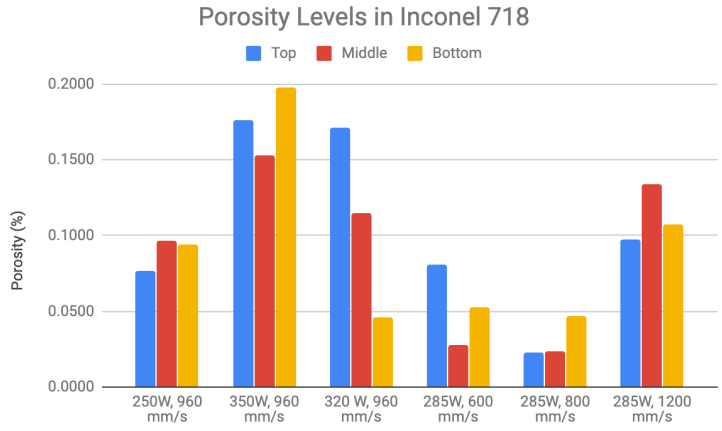

Figure 1: This figure shows the porosity values at each section of 6 different Inconel 718 samples.

Conclusions:

We were able to successfully analyze the quality of our analysis techniques on both CMSX-4 and Inconel 718. We will be designing biocompatible parts in the future using both Ti64 and Co-Cr and apply these techniques to determine whether or not the part is biocompatible.

Acknowledgements:

I would like to thank Professor Anthony Rollett, Dr. Amir Mostafaei, and Samuel Passell for helping me characterize the builds and analyze its microstructure. I would also like to thank the Biomedical Engineering Department for funding my research.

Fibronectin Nanofiber-Patterned Collagen Scaffolds For Engineering Aligned Cardiac Sheets

Xining Gao[1], Jacqueline Bliley[1], Rachelle Palchesko[1], and Adam W. Feinberg[1]
[1]Carnegie Mellon University

Introduction: The heart is an organ that is of high interest in the field of regenerative medicine because it has limited capacity to regenerate following injury. Current approaches to engineering 3D heart tissue include casting hydrogels with heart muscle cells (aka cardiomyocytes). These, however, often fail to fully recapitulate the native structure of the heart. Cardiac tissue consists of layers of anisotropic myocardial sheets, organized to increase contractility of the cardiac muscle, which is necessary to support its pumping ability. The extracellular matrix (ECM) is imperative in directing this cellular organization due to its highly aligned structure, making it essential to recapitulate this organized architecture when engineering cardiac tissue. This project seeks to develop a scaffolding to engineer highly aligned cardiac tissue from the bottom up, using fibronectin line micropatterns on collagen hydrogel sheets. Our goal is to eventually create a 3D tissue by stacking these aligned, 2D layers of cardiac tissue.
Materials and Methods: Compressed collagen I hydrogels were fabricated using a procedure described by Palchesko et al[2] and patterned with 20 μm wide fibronectin lines, spaced 20 μm apart (20x20). To carry out the hydrogel patterning, the fibronectin lines were microcontact printed onto a 2% high molecular weight poly(N-isopropylacrylamide) surface using a polydimethylsiloxane stamp, then transferred onto gelatin, and finally transferred onto the collagen. Successful transfer of the fibronectin pattern was confirmed by imaging the fluorescently labeled fibronectin with a confocal microscope. Human embryonic stem cell-derived cardiomyocytes were seeded on these patterned substrates at a density of $3x10^5$ cells/cm^2. Samples were stimulated in Tyrode's solution with paired platinum electrodes. To prepare for stimulation, a rectangular flap (~2 mm by 4 mm) was cut in each sample. Samples were then stained for DAPI, phalloidin, and α-actinin and imaged with a Zeiss LSM700 laser-scanning confocal microscope to assess cardiomyocyte attachment.
Results and Discussion: Fibronectin patterns were transferred onto the collagen hydrogels with high fidelity (Fig. 1a). It was observed that both line spacing and line width were accurately preserved in the patterning process. The cardiomyocytes were in culture for 5 days after seeding on the patterned collagen substrates. It was observed that, upon stimulation, the cardiomyocytes generated enough contractile force to deflect the collagen substrate (Fig. 1b & 1c). Subsequent fluorescent imaging verified that the cardiomyocytes successfully attached to and grew on the substrates, based on the presence of sarcomere banding and α-actinin expression. Furthermore, the cardiomyocytes appear to be aligned with the fibronectin pattern (Fig. 1d).

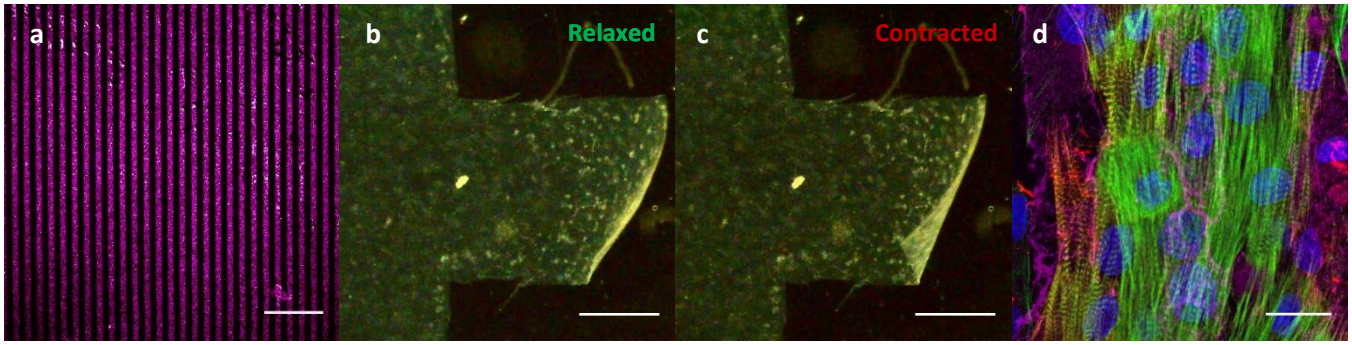

Figure 1. (a) 20x20 fibronectin line pattern on collagen hydrogel. Scale bar: 200 μm (b-c) Contracting cardiac sheet during stimulation with relaxed sheet shown in (b) and contracted sheet shown in (c). Scale bars: 200 μm.
(d) Cardiomyocytes on patterned substrate. Blue: DAPI, green: phalloidin, red: α-actinin, pink: fibronectin. Scale bar: 20 μm.

Conclusions: We demonstrate the capability to successfully pattern collagen I hydrogels with fibronectin, seed the hydrogels with cardiomyocytes to form aligned 2D cardiac sheets, and stimulate the cardiomyocytes to bend the collagen substrate. Future work will quantify cardiomyocyte alignment on the fibronectin lines and contractile force generation of these cardiac films. After these steps, we will stack the 2D cardiac sheets to create 3D tissue structures.
Acknowledgements: We would like to thank the Carnegie Mellon University Department of Biomedical Engineering and the American Heart Association for their support.
References: [1]Feinberg AW. Science. 2007. 317(5843):1366-70. [2]Palchesko RN. Advanced Healthcare Materials. 2016. 5(22):2942-50.

Developing Non-Contact Functional Near Infrared Spectroscopy for Brain Imaging

Authors: J. Cortes, W. Scammon, J. Yang, A. Ruesch, C. Robbins, JM. Kainerstorfer
Carnegie Mellon University, Department of Biomedical Engineering

Introduction: Function near infrared spectroscopy (fNIRS) is a non-invasive imaging method where near infrared (NIR) light is sent from a source into tissue. The NIR light diffuses through the tissue causing a fraction of the photons to return to the surface which are fed to a detector at some distance away from the source. Oxygenated hemoglobin and deoxygenated hemoglobin in blood absorb different wavelengths of NIR light. Using coupled wavelengths of NIR light and the modified Beer-Lambert law it is possible to calculate how many photons were absorbed and thereby determine changes in hemoglobin concentration. Currently in fNIRS both source and detector are placed ipsilaterally on the tissue of interest. The study aims to show that it is possible to detect changes in hemoglobin concentrations while having a non-contact detector. This can lead to a better non-invasive method of measuring changes in hemoglobin concentration in people as well as improvements and innovations in how and where fNIRS is used.

Materials and Methods: Phantoms made out of silicon and titanium oxide where used to mimic brain tissue. The phantoms had hollow channels of varying depths ranging from 2-20 mm that served as pathways for indigo ink to pass through. Indigo ink flowed through the channels in order to mimic absorption in neural activity. A 785 nm NIR laser of a multi-channel fiber coupled laser module [MCLS1, Thorlabs] was used as the source to emit the NIR light which was guided using a 785 nm fiber [M42L02, Thorlabs]. The ProEM HS: 512BX3 EMCCD camera [Princeton Instruments] was used to take 512 by 512 pixel images of the incoming photons in order to detect multiple source-detector distances. The source light was sent through a collimator [F220FC-780, Thorlabs] to focus the incoming light beam and send the greatest amount of photons into the phantom. The collimated source and detector were cross polarized using two linear polarizers [LPNIR100-MP2 ,Thorlabs] in order to eliminate surface reflections. The source and detector were kept a constant 38 mm above the phantom. Trials were done at each varying channel depth with multiple images collected per trial. The images were separated into two groups, no ink flow, and ink flow. For each trial, each of the image groupings were averaged together to reduce noise and create an average image of no ink flow or ink flow. The average image of ink flow was subtracted from the average image of no ink flow which resulted in an image displaying changes in light intensity due to absorption of the ink.

Results and Discussion: Light absorption changes were detected at depths of 2-16 mm as shown in Figure 1, to a point where the channel can be detected and its effect shown around the channel. The deeper the light travels the less photons are detected by the camera causing for resolution drops corelated to channel depth.

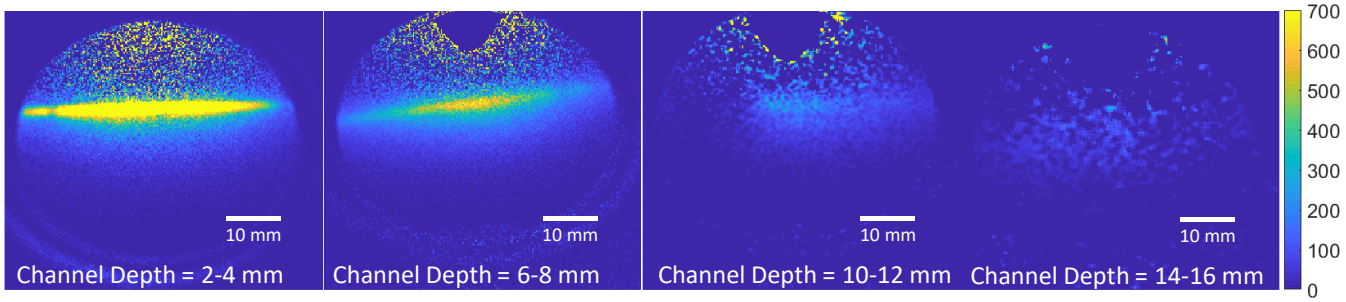

Figure 1: Yellow areas represent sections where large amounts of light were absorbed. Light blue areas show smaller amounts of absorption. As depth increases less light absorption is detected. The image for channel depths 10-12 and 14-16 mm were passed through a median filter to remove noise.

Conclusions: Light absorption changes can be detected using a non-contact fNIRS system setup at 2-16 mm deep phantoms. Our data suggests that non-contact fNIRS can potentially detect absorption changes through the human skull at surface level brain activity. Therefore we have shown that non-contact fNIRS should be possible. We are planning to run in vivo measurements of functional brain activation in the future.

Acknowledgements: The project was funded by the Air Force Office of Scientific Research. The Carnegie Mellon BME SURP program made this summer research project possible.

Modeling the Melanoma Microenvironment with Spheroid Cocultures

Augustine Duffy[a,b], Andrew Bradshaw[c], Howard Edington[b,d], and Alan Wells[c]
[a] Department of Chemical Engineering, Carnegie Mellon University
[b] Department of Biomedical Engineering, Carnegie Mellon University
[c] Department of Pathology, University of Pittsburgh
[d] Department of Surgical Oncology, Allegheny Health Network

Introduction: The tumor microenvironment (TME) has been shown to play a major role in the development of cancer through mechanisms such as the inhibition of growth suppressors and inactivation of apoptotic signals [1]. Additionally, the TME may play a critical role in promoting and enabling metastasis from the primary site and in conferring therapeutic resistance for both primary and metastatic tumors [2]. Thus, understanding the contribution of each component of the TME towards tumor aggression and resistance could enable the re-sensitization of tumors to current treatments and/or the development of new therapies. Unfortunately, most current *in vitro* tumor organoid models lack an intact TME and thus cannot be used for these studies [3]. However, tumor and cancer-associated fibroblast (CAF) cocultures have shown promise at recapitulating the TME [3]. Here, we extend that model by incorporating monocytes to further capture the cellular heterogeneity of the TME. We then use our model to investigate the contribution of CAFs towards tumor aggression.

Materials and Methods: GFP-expressing melanoma cells A375 (malignant) and WM1158 (metastatic) were used as the model tumor cell lines. Spheroid cocultures were formed by seeding tumor cells, DiI-stained THP-1 monocytes, and either CAFs or normal fibroblasts into low adhesion culture wells. Cocultures were incubated for 72-96 hours, and spheroid homogeneity was then verified using fluorescence microscopy. Intact spheroids were embedded into collagen I matrices and imaged each day for three days.

Results and Discussion: Both CAF and non-CAF spheroids indicated successful mixing of tumor cells, monocytes, and fibroblasts (Figure 1A). Embedded spheroids also demonstrated visible outgrowth over three days of incubation (Figure 1B). Unfortunately, small sample sizes due to incomplete embedding in the collagen matrix prevented significant conclusions from being drawn from our results. Additionally, large variations in spheroid outgrowth were observed among samples with the same conditions, indicating that additional factors may be influencing spheroid outgrowth.

Conclusions: We demonstrated that homogenous spheroids containing tumor cells, monocytes, and fibroblasts could be successfully generated and that those spheroids demonstrated visible outgrowth over three days of incubation. Additional trials are needed, however, to conclusively determine the effect of CAFs on tumor outgrowth within this model and to determine the cause of the large variability in outgrowth among samples under the same conditions. Furthermore, additional cell types, such as adaptive immune cells or mesenchymal stem cells, can be incorporated into future models to further approach the cellular heterogeneity of the TME.

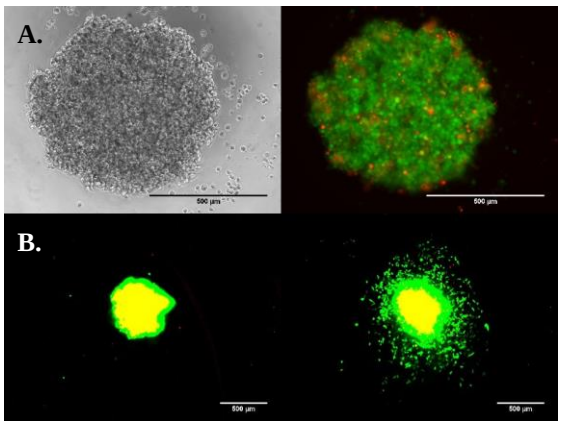

Figure 1. Spheroid modeling of the melanoma TME. (A) Spheroid homogeneity was verified by fluorescence microscopy. Green: A375 melanoma. Red: THP-1 monocytes **(B)** Outgrowth of CAF-containing spheroid from Day 0 (left) to Day 3 (right). Green: WM1158 metastatic melanoma. Red: THP-1 monocytes.

Acknowledgements: We would like to thank Dr. Alan Wells and Dr. Howard Edington for their advice and assistance. We would also like to thank Erica Kuo (Department of Pathology, University of Pittsburgh) for her help in spheroid preparation. This project was funded in part by the Summer Undergraduate Research Program of the Department of Biomedical Engineering at Carnegie Mellon University.

References:

1. Pickup, M W, *EMBO Rep*, 2014, 15, 1243–1253.
2. Wells, A, *Exp Biol Med*, 2018, 243, 1243–1253.
3. Tuveson, D, *Science*, 2019, 364, 952–955.

Stepping Back by Stepping In: The Importance of Clinical Immersion in Senior BME Design

Authors: Olivia Olshevski & Julia Salerno

Introduction: Capstone design projects are an essential part of the biomedical engineering curriculum. While this curriculum provides the skills necessary to design and create a biomedical device capable of solving an unmet need in today's clinical environment, determining which needs to focus on is crucial to the project's success. Carnegie Mellon's Clinical Immersion Fellowship (CIF) commits substantial time and energy to this critical step in the biodesign process[1] while remaining mindful of the limited clinical exposure most undergraduate students receive. By bringing a select number of dedicated students into direct contact with medical personnel, CIF takes a hands-on, immersive approach to clinical needs-finding that produces meaningful solutions grounded in local, real world problems. In the program's third year, CIF has grown to include more clinical contacts and shown a marked increase in productivity, identifying 26 potential projects (compared to 7 in its first year and 10 in its second).

Materials and Methods: CIF fellows took a holistic, observation-based approach to identifying unmet needs in a variety of medical environments. Prior to each immersion, fellows performed background research on potential focus areas, such as physical & occupational therapy, cardiothoracic & neurosurgery, and common medical emergencies. During observations, fellows took notes by hand and employed the AEIOU observation design method[2], focusing on activities, environments, interactions, objects, and users within each clinical setting. Where appropriate, CIF fellows also spoke with both patients and medical personnel to acquire multiple perspectives. After each day of observation, fellows created an extensive list of identified needs, and these lists were then combined into an initial draft of ideas. Fellows then used the scope and skill sets of the senior design class as criteria for parsing the draft into a final catalog of potential projects. Each project in this catalog was further developed into an accompanying write-up describing the scope of the problem, target population, and desired outcome.

Results and Discussion: The initial draft contained 26 ideas gathered from 7 departments across 3 institutions: Foxwall EMS, Allegheny General Hospital (AGH), and The Children's Institute. At Foxwall, fellows shadowed crew members during calls throughout a 2-week period, for a total of 40 hours. At AGH, fellows observed multiple procedures in the cardiothoracic and neurosurgery departments across a 12-hour, 2-day span, and at the Children's Institute, fellows attended physical, occupational, locomotive, and speech therapy appointments during a single 8-hour work day. Of the initial ideas, 15 were selected as potential design projects, and a few others, while interesting, fell outside the scope of the undergraduate design course. This more advanced collection will be shared with both the graduate BME design class and other engineering departments.

Conclusion: Though future iterations of the program should focus on establishing earlier communication with clinicians to increase the number of days spent observing, CIF's influence is three-fold: it 1) builds and sustains relationships with local medical personnel, thereby enabling our department to continue to manufacture fruitful products with meaningful, real world impacts, 2) serves as a compromise between the little clinical exposure provided to undergraduates and the importance of immersive, observation-based design, and perhaps most importantly, 3) allows students to define and investigate problems that they care about. More personal than hands-off research to solve problems brought to us by big name companies, Carnegie Mellon's CIF gives agency back to students and allows the design class to return to the purest form of engineering: finding and fixing a problem entirely on your own.

1 Krummel, Thomas M., et al. *Biodesign: The Process of Innovating Medical Technologies*. Cambridge University Press, 2017.

2 Martin, Bella, and Bruce M. Hanington. *Universal Methods of Design: 100 Ways to Research Complex Problems, Develop Innovative Ideas, and Design Effective Solutions*. Rockport Publishers, 2012.

Flexible Adhesive Strain Sensors to Monitor Cardiac Output

Authors: Bryant J. Chung, Chenchen Mou, Christopher J. Bettinger
Departments of Materials Science and Engineering and Biomedical Engineering, Carnegie Mellon University, Pittsburgh, PA

Introduction: Cardiovascular shock is a drastic change to cardiac patients' performance post-operation and accounts for a 38% mortality rate post-operation. [1] Current methods of detecting cardiovascular shock use invasive pulmonary artery catheters, which come with varied risks such as arterial punctures, infection, and thrombus formation. [2] The ideal approach to measure cardiac output would provide identical information of heart function, but at much lower risk to the patient. To this end, we designed and fabricated flexible adhesive epicardial sensors that can measure cardiac output while presenting the patient with minimal risk. Specifically, measuring the strain of the aorta using flexible hydrogel-based strain sensors can give insight into hemodynamics to ultimately assess cardiac output. Here we describe the design, fabrication and calibration of hydrogel-based flexible strain sensors.

Materials and Methods: The Au structures used as the primary strain sensor were fabricated on a silicon wafer using standardized photolithography and thin film deposition techniques. [3] A sacrificial layer of polyacrylic acid (PAA) was deposited on the Si prior to Au deposition onto the wafer, allowing for easier liftoff of the complete Au structure via the hydrogel. The hydrogel was comprised of $FeCl_3$ dissolved in tris buffer solution mixed with the $[(PEG\text{-}Cat)_4]$ polymer which was also dissolved in tris buffer. Hydrogel precursors were deposited on Au microstructures on Si wafers and incubated for 90 minutes in a sealed environment; this allowed for the Fe^{3+} ions to cross-link with the $[(PEG\text{-}Cat)_4]$ tails in the polymer solution. [3] These hydrogels were then integrated with a polydimethylsiloxane (PDMS) strip and strained, simulating both the mechanics and strain of the aortic arch. [3] The resistance of the hydrogel was recorded as a function of strain.

Results and Discussion: Two aspects of the hydrogel formation process were controlled: the concentration of the $[(PEG\text{-}Cat)_4]$ polymer and the ratio of Fe^{3+} ions present in the hydrogel to said polymer. The best formulation of hydrogel tested had a $[(PEG\text{-}Cat)_4]$ polymer concentration of 40 mM and a Fe^{3+}:catechol ratio of 0.4. The low concentration of polymer allows for a slower cross-linking time between the Fe^{3+} ions and the catechol tails in the polymer; the low Fe^{3+}:catechol ratio allows for a softer hydrogel for stronger integration with the PDMS substrate for strain testing. The results of straining the device are shown below in Figure 1. The figure shows how linear the device is in the lower percentages of strain, meaning that its sensitivity as a strain sensor is high. Furthermore, the response is fairly linear up to about 17%, a dynamic range that is appropriate for our intended application.

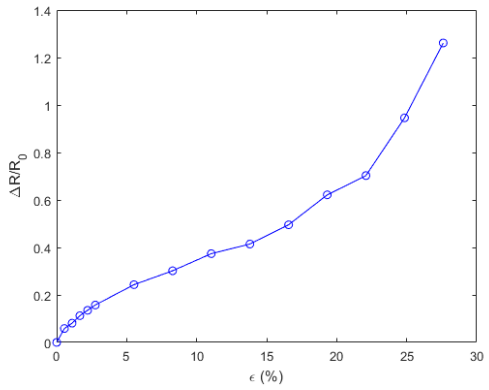

Figure 1. Hydrogel Formation and Strain Testing. This graph shows how exactly the resistance changes as a result of applied strains. This sample was measured for how its resistance changed as the PDMS was strained underneath it (which also strained the attached hydrogel with Au pattern on top). As the resistance of the sensor changes with applied strains, the graph climbs linearly as desired, but after the 23% mark, the relationship becomes exponential in nature, which is undesired for aortic applications. A larger linear relationship would allow for direct correlations between the strain applied and the resistance of the device; this ambiguity warrants further investigation.

Conclusions: The Au nanostructures' initial resistance tests are showing resistance trends that proportionally follow the increase of strain to a certain degree. Future studies will involve further developing the linear relationship between the electrical resistance and the strain applied to the hydrogel. Being able to extend the range of linearity of the device would create a better sensor for this application.

Acknowledgements: B. J. Chung would like to acknowledge his team members Nathan Roblin and Adrian A. Johnson for their continued help with data acquisition and analysis, and the Carnegie Heart Program for hosting him for the summer, led by Prof. Keith Cook and Prof. Xi Ren and funded by the American Heart Association.

References: [1] Mebazaa, A.; et al. *Crit. Care* **2010**, *14*:201 [2] Wiedenroth, C. B.; et al. *Jour. Throm. Throm.* **2017**, *44* (3), 335. [3] Huang, W.-C.; et al. *Adv. Funct. Mater.* **2016**, *28*, 1801059.

Microfluidic Study of Clot in an Artificial Lung

Author: Sarah Hargett, Carnegie Mellon University Departments of Chemical and Biomedical Engineering

Introduction: With over 15 million Americans suffering from pulmonary diseases such as chronic obstructive pulmonary disease and cystic fibrosis and an immense shortage of available lung donors, the need to find alternative treatment options is critical. One alternative involves the use of extracorporeal membrane oxygenation, or ECMO, which employs an oxygenator device to either replace or support the body's natural lung function. ECMO is effective in the short term as a rescue therapy; however, clot formation inside the device reduces blood flow and prevents gas exchange, requiring the replacement of the oxygenator within four weeks. This research project aims to improve understanding of how the physical structure of an ECMO oxygenator affects clot formation, with the ultimate goal of informing the design of future oxygenators.

Materials and Methods: Microchannels that mimic the design of an ECMO oxygenator are 3D printed using digital light projection stereolithography. The devices are designed with varying specifications for the path length (2 cm and 4 cm) and hollow fiber packing density (40%, 50%, and 60%) to mimic the ranges seen in clinical oxygenators. The devices are incorporated into a small circuit including a syringe, syringe pump, and manometer for a benchtop experiment. Whole human blood is perfused through the device, with added heparin to simulate varying thrombogenicity in clinical conditions (aPTT: 25-45 s). Frontal area (80 cm^2, 100 cm^2, and 120 cm^2) of a clinical device is modeled by scaling the blood flow velocity. Following the experiment, any unclotted blood is rinsed out. To quantify clot, the pressure drop across the device is recorded during the experiment and the device is weighed before and after the experiment. The devices are also imaged using microCT scanning to determine the volume of clot within the device. The goal of this experiment is to determine which design variations tend to produce the least amount of clot, and so analyzing this data can help elucidate such a relationship.

Results and Discussion: Preliminary results suggest that a packing density of 40% may be the best variation, as this device produced the least amount of clot, at 0.137 g (N = 1) and the smallest increase in pressure, with a maximum of 0.7 mmHg increase. A frontal area of 80 cm^2 produced the least clot measured via mass, at 0.043 ± 0.066 g (N = 5), but does not appear to be correlated with clot formation according to pressure measurements thus far. A path length of 2 cm produced the lowest amount of clot measured via mass, at 0.162 ± 0.040 g (N = 3), but the 4 cm device produced the smallest increase in pressure, with a maximum pressure at 2.07 ± 1.82 mmHg (N = 3). The data will be further analyzed using microCT scanning and digital image processing to better determine clot formation in terms of volume. A preliminary example of this analysis is shown in figure 1.

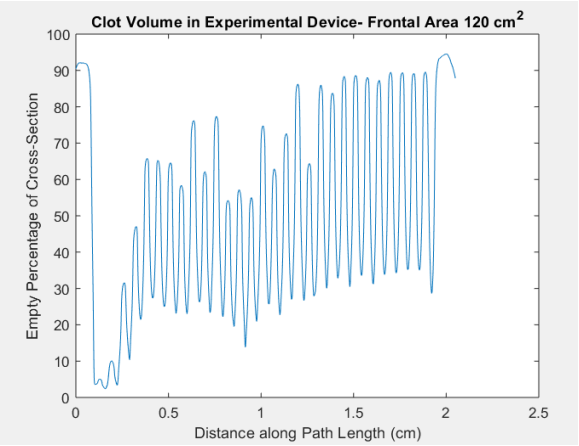

Figure 1. Analysis of microCT scan data for an experimental device. Oscillations in graph correspond with internal structure of device and will be removed in future analysis.

Conclusions: Preliminary data indicates that a decreased packing density and increased path length produce the least amount of clot inside the device. Results thus far do not indicate a correlation between the frontal area and clot formation. Additional trials will be conducted for each of the design specifications.

Acknowledgements: This research project was made possible by the Biomedical Engineering Department of Carnegie Mellon University, Allegheny Health Network, and the American Heart Association. The author also thanks PhD candidate Angela Lai and Dr. Keith Cook for their time and guidance with this project.

Optimization of Magnetic Field Strength for Cardiac Magnetic Resonance: A Case for .75T Low Field Imaging

Mimi (Xinyi) Li

Introduction:

Recent developments in Cardiac MRI (cMRI) imaging techniques have widely reduced scan times at the expense of imaging quality as indicated by lower Signal-to-noise ratios (SNR). In order to recover the lost SNR, there has been a push towards developing higher field systems due to the idea of there being a linear relationship between field strength and SNR. In the past decade, experts were hopeful that 3T imaging for cMRI would become the standard in the coming years, however, several drawbacks have emerged. One limitation is the increased Specific Absorption Rate (SAR) that could result in heating of the patient's tissues. Another major limitation is that at higher field strengths, greater image inhomogeneity and artifacts can occur which severely distort the image. However, these limitations are virtually nonexistent at low fields-- the only question becomes, whether or not a sufficient SNR can be generated. One such method is by manipulating the Repetition Time (TR) which is the time between radio-frequency pulses in the scanner; longer TRs allow narrower bandwidths (BW) to lower noise, but at the expense of making the image more sensitive to susceptibility artifacts. With the benefit of high absolute homogeneity at low fields, using a longer TR is possible, allowing for reduced receiver BW which introduces less noise into the signal, thus resulting in a higher SNR without higher artifacts. Ultimately, the objective of this study is to investigate the optimal field strength while maintaining or potentially improving high quality diagnostic imaging.

Materials and Methods:

Measurements were performed on an agar phantom, which emulates the relaxation characteristics of the myocardium, using a clinical whole body 1.5T MRI system to produce steady state free precession images. A theoretical expression for SNR was derived and compared to the SNR of the phantom images acquired at various matrix sizes, BWs, NEX values in order to confirm the validity of the expression. To simulate the SNR at various field strengths, characteristics of the scans such as TR and BW, as well as acceleration factors developed by the lab were parameterized. The parametrized components were then used in the theoretical SNR equation to model SNR at low fields ranging from .1T to 1.7T using a constant breath hold of 16.7s and the 1.5T 224^2 matrix scan as the reference.

Results and Discussion:

Comparison of the expected theoretical SNR with the experimental SNR using the scans of the imaging phantom, yielded a linear line with an R^2 value of 94.9%, thus confirming that the SNR model developed is a good fit for the phantom data. The equation was then used to model the SNR of different field strengths relative to the 224^2 matrix at 1.5T standard scan. The optimal field strength was found to be a broad plateau centered on 1T for both the standard resolution 224^2 matrix and the higher resolution 384^2 matrix. Despite the SNR being lower for the higher resolution, it is still within the range that is widely accepted today for parallel imaging.

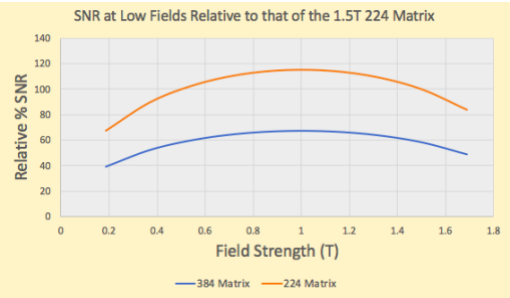

Figure 1. SNR at low fields of differing imaging resolutions using a 224^2 and 384^2 imaging matrix relative to a 1.5T, 224^2 matrix standard scan.

Conclusions:

The SNR achievable is higher at low fields of .75T-1T for standard imaging with a 224^2 matrix, rendering the SNR of the 1.5T machines widely used in cMRI today suboptimal. Additionally, higher image resolutions using a 384^2 matrix are obtainable at lower fields with respect to generation of imaging artifacts and no realistic limitation on SAR since it is reduced as field strength decreases. Further work can be done to explore the effects of 3D imaging, which is known to greatly improve SNR. Indeed, the idea that higher fields automatically means higher quality images is far from accurate.

Acknowledgements:

I would like to thank Dr. Mark Doyle and Dr. Robert Biederman for their knowledge, guidance, and support on this research project.

Title Should Be Typed in Initial Caps

Authors: GianCarlo Seixas, Jooli Han, and Dennis R. Trumble, PhD

Introduction:

Congestive heart failure (CHF) remains one of the most costly diseases in the industrialized world, both in terms of healthcare dollars and the loss of human life. Despite great strides made in the treatment of CHF using mechanical ventricular assist devices (VADs), longstanding difficulties associated with percutaneous driveline infection and clot formation at the blood-device interface has limited their long-term use. Our lab is working to develop a self-contained, non-blood-contacting VAD that bypasses these limitations using an internal muscle energy converter (MEC) to drive a non-blood-contacting direct cardiac compression sleeve (DCCS).[1] Taking into account the natural anatomical and hemodynamic differences between the two sides of the heart, we are now working to refine and improve this approach for long-term circulatory support via computational simulations of DCCS dynamics.

Materials and Methods:

The active element of this compression device is an array of thin-walled polymer tubes connected side-by-side and wrapped around the heart. As fluid enters the empty tubes, they transform from an elliptical to a circular cross-sectional configuration, effectively decreasing the widths of the tubes and, in turn, the radius, size, and enclosed volume of the DCCS device. By adjusting the size and number of tubes, device actuation profiles can be modified to maximize the level of achievable cardiac assistance. Here, characterization and validation of device function has been performed *in silico* through finite element analysis (FEA) in preparation for device fabrication and *in vitro* performance testing.

Results and Discussion:

Four fundamental geometric constraints regarding tubular inflation dynamics have guided the overall optimization process to this point. First, as the size of the polymer tubes increases, device stroke volume (SV) increases, leading to greater cardiac compression. Second, as the number of tubes increases, dimensional constraints decrease maximum SV. Third, as the size and number of tubes increases, the total hydraulic volume (HV) required to actuate the device increases. And fourth, smaller tubes provide greater potential volume amplification (SV/HV). In addition, the MEC itself places both a pressure (< 0.36 MPa) and a hydraulic volume (<15 mL) constraint on device actuation while device actuation cycles must be designed to produce equal volume outputs from both ventricles.

Optimization of the device called for a constrained multivariate optimization program, written in Python, ensuring SV is maximized without breaching any dimensional, physiological, or manufacturing constraints. It was found that stroke volumes up to 38.5 mL are theoretically achievable via this mechanism. However, FEA showed that portions of the device with smaller tubing were unable to actuate under allowable MEC pressures. Adjusting the minimum tubing size, it was found that visible compression could occur with larger tubing but would subsequently reduce maximum device SV.

Conclusions:

The development of a completely implantable muscle-powered DCCS has the potential to be a useful device in aiding cardiac function while avoiding current VAD limitations. Manipulation of device geometry, notably the size and number of tubes on the device, has led to improved theoretical cardiac compression profiles. However, an optimal device design has yet to be established and validated. Further studies are needed to ensure that device SV is truly maximized, after which the device will be manufactured and tested on the bench to validate its function.

References:

1. Han, J., Kubala, M. & Trumble, D. R. Design of a Muscle-Powered Soft Robotic Bi-VAD for Long-term Circulatory Support. in V001T01A003-V001T01A003 (American Society of Mechanical Engineers, 2018). doi:10.1115/DMD2018-6835

Sonication of Silk Microspheres for Controlled Drug Delivery

Isabelle Chickanosky[1], Megan DeBari[1], Dr. Rosalyn Abbott[1]
Carnegie Mellon University[1]

Introduction: Targeted drug delivery is an essential aspect of the medical field that works to maximize the efficiency of medications while also minimizing the negative systemic side effects that can follow non-targeted drug exposure. Many methods of targeted drug delivery are catered for individual symptoms, but this can lead to difficulty in specificity and production of the medication. This proposed method of drug delivery would allow for drug release to be triggered by therapeutic ultrasound, so drug capsules could circulate through the blood and release the medication only in the desired location of sonication. Silk fibroin serves as a useful material in biomedical applications due to its biocompatibility, biodegradability, and tunable mechanical properties [1], which qualifies it to be the capsule of the proposed drug delivery mechanism. Controlled degradation of silk microspheres will allow for new non-invasive drug delivery methods. Such methods will target specific regions of the body, minimizing the negative side effects associated with conventional drug delivery by decreasing the drug concentration throughout the body. Ultimately, the success of this research will open new doors for the use of silk fibroin as a drug delivery tool.

Materials and Methods: *Bombyx mori* silkworm cocoons were processed to a silk fibroin liquid solution. As described previously, silk microspheres were made by combining silk solution with a lipid, DOPC, by a series of steps including lyophilization and centrifugation [1]. During this process, the fluorescent dye, green fluorescent protein (GFP), was enveloped by the silk microsphere as a method to determine if the sonication process could burst the microspheres. To determine consistency between microspheres being made, some were sampled for size by using the Malvern Nano Zetasizer, some were sampled for structure by imaging with the Explorer Scanning Electron Microscope, and others were exposed to therapeutic ultrasound then examined in a UV-Vis spectrometer to determine the effectiveness of the ultrasound degradation of the silk microspheres.

Results and Discussion: The first step in understanding the potential of silk microspheres as drug capsules was to create silk microspheres that could successfully form around water. Figure 1A shows that silk microspheres can carry a drug, providing a successful capsule. The micrographs from the SEM also revealed the successful production of silk microspheres carrying GFP, as can be seen in Figure 1B. Sonication of the GFP loaded silk microspheres demonstrated the release of GFP that was not statistically greater than controls. Future work will involve increasing sample sizes to improve statistical power and standardizing the size and number of GFP microspheres to quantify drug releasing characteristics.

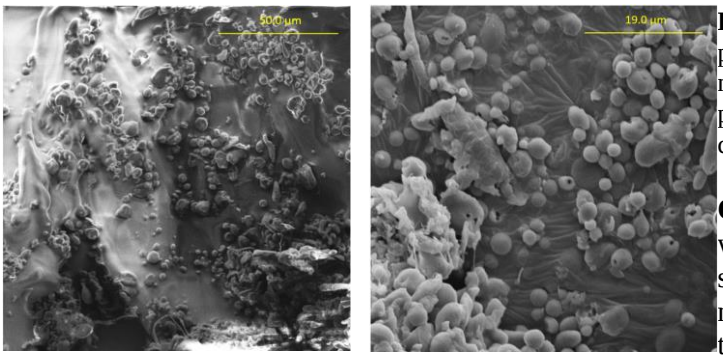

Figure 1. (A) Image of silk microspheres produced using water ranging from 2 to 10 microns. (B) Image of silk microspheres produced using GFP to simulate their ability to carry a drug ranging from 2 to 10 microns.

Conclusions: Consistent with other work, it was determined that silk microspheres can successfully carry a drug as a capsule. Silk microspheres are highly stable and can last in the body for months. Furthermore, the initial release of GFP from silk microspheres provides potential to trigger degradation silk microspheres using therapeutic ultrasound.

Acknowledgements: This work was supported by the BME Department at Carnegie Mellon University.

References: [1] D. N. Rockwood, *Nat Protoc*, 2011, vol. 6, no. 10, pp. 1612-31